Attitude dynamics and control of a large flexible space structure by means of a minimum complexity model

Francesco Nicassio[a], Daniele Fattizzo[b], Michele Giannuzzi[a], Gennaro Scarselli[a,*], Giulio Avanzini[a]

[a]*Department of Innovation Engineering, Ecotekne Campus, Building O, Lecce, 73100, Italy,*
[b]*Department of Industrial Engineering, University of Bologna, Alma Mater Studiorum, Bologna, 40126, Italy,*

Abstract

A technique for deriving a low-order model of a large, deformable space vehicle, with a configuration resembling that of the International Space Station, is proposed. The modeling approach is based on a hybrid Newtonian-Lagrangian approach, where a generalized Euler equation is written for rotational degrees of freedom, whereas the dynamics of states associated to deformation by means of a Galërkin approach is derived by means of a Lagrangian formulation. The assumed modes method is adopted, where modal characteristics of the main deformable structure are estimated on the basis of its real characteristics, estimated by means a finite element model of the actual truss configuration. A cluster of control moment gyroscopes is considered as the actuator for attitude control. Open- and closed-loop maneuvers are considered, in order to highlight coupling between rotational and deformation degrees of freedom. The modeling tools allows for a quick search of gains which minimizes structural excitations during large angle slews.

Keywords: Flexible space structure, Attitude control, Low-order models.

1. Introduction

The objective of the paper is to derive attitude control laws for large flexible space structures, evaluating the resulting excitation of deformation

*Corresponding author
Email address: gennaro.scarselli@unisalento.it (Gennaro Scarselli)

Degrees of Freedom (DoFs) during and at the end of large angle reorientation maneuvers. The attitude control of a flexible space system has been investigated in many research papers and reports, such as [1, 2, 3]. As an example, Malla and Lin established an orbit-attitude-structure coupled model, based on an absolute nodal coordinate formulation, which is accurate in modeling rigid-flexible coupled effects and large-deformation cases [4].

The motivations for this research are mainly two, both related to the extreme pointing precision required by some scientific payloads. First of all, when these payloads are installed on board of a spacecraft, active or passive supports with vibration isolation capabilities are often required, for reaching the pointing precision specified by mission requirements. Hence, a reasonably accurate knowledge of vibrations induced by attitude maneuvers is crucial in designing the payload support system [5]. Quite obviously, vibration isolation/suppression systems (as in [6]and [7]) represent a penalty in terms of additional cost and weight, and, for active ones, complexity (in this latter respect harming overall system reliability). As a consequence, a second objective for the research becomes relevant, namely the search for attitude control laws which minimize structure excitation [8]. By accurately selecting control laws and gains, it may be possible to avoid the need of active vibration control, if residual vibrations are brought below an acceptable threshold [9]. The work aims at providing the community with a physically consistent approach for the derivation of low-order models [10] of large deformable space structures, demonstrating the viability of the method in the framework of control law synthesis for large angle reorientation maneuvers.

The reduced order model presented in the paper is indeed useful for didactic purposes, highlighting coupling between all three rotational DoFs and deformation variables in a simplified, yet realistic, scenario. Nonetheless, the proposed approach is significantly more complex and complete than the derivation of single-axis models, like that presented in the book by Junkins and Kim [11]. The low-order model developed can thus also be used for the synthesis of control laws which minimize excitation of deformation DoFs during fast, large angle slews at a very early stage in the design process. In this framework, the availability of a simplified model requires a small number of relevant parameters, hence it allows for such an activity prior to the exact definition of the actual structural properties. Moreover, model parameters representative of global characteristics of the structure can be easily updated in the presence of more detailed information on the actual properties of the flexible spacecraft. To the best of the authors' knowledge, such a model is

not yet available in the technical literature.

Attitude dynamics and control of large space structures [11, 12] pose several challenges, which make the problem far from trivial [13]. On the modeling side, in the presence of large attitude variations coupled with local deformations, a hybrid system of nonlinear ordinary differential equations (governing rotational dynamics) and partial differential equations (ruling deformation degrees of freedom) is derived in [14] and [15]. Moreover, the determination of deformation modes for large structures made of elements of different type (trusses, panels, pressurized elements, joints, etc.), may result into high order models, when a classical Finite Element Method (FEM) is adopted [16]. Such models are not suitable for control law synthesis.

On the other hand, control or large orbiting bodies poses additional challenges, especially in the presence of saturation phenomena, which limit the maximum angular acceleration (because of bounds on available torque) and angular rates (because of bounds on angular momentum stored in the cluster of spin wheels). The use of control moment gyroscopes (CMGs) as attitude effectors allows for performing zero-propellant attitude maneuvers [17, 18]. Unfortunately, in such a case, beside torque and angular momentum saturation issues, the intrinsic nonlinearity of the problem, and, more importantly, the presence of singular configurations for the CMG cluster [19] pose additional challenges to the control problem.

When a singular CMG cluster configuration is approached, gimbal control rates may diverge to unfeasibly high values, and the control effectors loose effectiveness, provided that in a singular configuration the system becomes underactuated, apparent gyroscopic control torque being constrained on a plane, perpendicular to the singular direction [19]. At the same time, deformations excited during the transient phases of the maneuver may induce oscillations, which may persist after reorientation is completed, if structural damping is low [11, 20].

Clearly, a simplified modeling approach may be extremely interesting, in order to provide enough information on deformation state during the attitude maneuver, while limiting overall system order, such that conventional control design techniques remain available with simple architectures [21, 22, 23, 24]. With this objective, a minimum complexity dynamic model of a large orbiting body, with size, mass distribution and configuration resembling that of the International Space Station (ISS) is derived, as a relevant test case for the envisaged technique. The model describes attitude dynamics of the vehicle, accounting for rotational DoFs and structural deformation, while keeping

model order low, by means of two strategies: (i) a simplified configuration is derived, where some elements of the vehicle are considered as rigid bodies attached to the deformable structure; (ii) deformation state is determined only for relevant variables by means of the assumed modes method [11], truncating the series expansion to a minimum number of modes.

As a preliminary step, a reduced order model of the truss is required, which reproduces (with acceptable accuracy) the dynamic behavior of the actual truss, which properties are determined by means of a Finite Element (FE) model. In this respect, a few studies are available, where FE methods are adopted for modeling and simulating the response of the entire ISS. As an example, the possibility of generating simple FE models of the first modules of ISS was studied in [25]. Alyaa [26] discusses the modal analysis for the Zvesda Mission of the Space Station using an alternative method, based on bond graph technology. In the present study, a truss which reproduces the geometry of that built for the ISS is accurately modeled by means of a FE method, in order to derive torsional and flexural frequencies and modal shapes. This study is then used for generating an equivalent Euler-Bernouilli beam, with the equivalent modal properties.

The procedure described in [11] for modeling single axis rotations of a cylinder with flexible appendages, based on the assumed modes method, is thus extended here to the case of a fully flexible large space structure with 3 rotational degrees of freedom, coupled with bending and torsional deformations. A hybrid Newtonian-Lagrangian approach is adopted [27]: a generalized Euler equation is written for describing the evolution of angular rate components of the deformable body, whereas the dynamics of deformation variables is derived by means of a Lagrangian formulation, under the assumption of small deformations.

The following section will provide the definition of structural models for the major elements of the ISS-like vehicle. An equivalent, low-order model for the main deformable truss of the vehicle is here presented. The derivation of a dynamic model of the whole vehicle, featuring relevant deformable elements and rigid appendages is provided in Section 3, where the attitude control problem is also formulated. Numerical simulations are discussed in Section 4 in order to analyze performance of closed-loop control laws for large angle slew maneuvers. The effect of control law gains on the resulting excitation of deformation DoFs is also studied. A section of concluding remarks ends the paper.

2. Modeling of a Large Space Structure

2.1. Geometry

Figure 1.a provides a pictorial representation of the International Space Station, where all the elements are clearly visible: a long truss, which represents the major structural element, a set of 8 pairs of orientable solar panels, placed at the edge of the truss, a group of pressurized modules, attached approximately in the centre of the truss, other minor elements, such as payloads, radiators, etc.

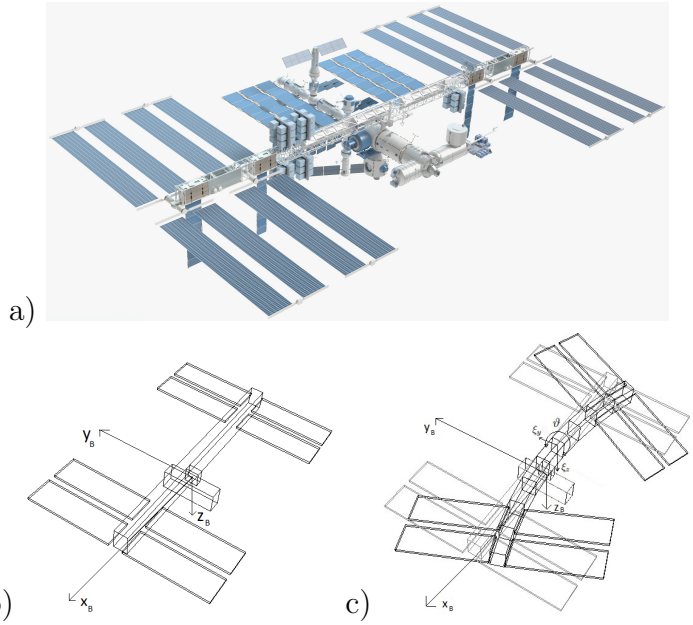

Figure 1: Sketch of the ISS configuration (a); equivalent vehicle in undeformed (b) and deformed (c) conditions.

A simplified scheme for the configuration is here adopted (Figure 1.b), where the only deformable element is the truss, whereas pairs of solar panels and the cluster of pressurized modules are treated as rigid bodies of known inertia, attached to the truss. Other elements of the original ISS configuration are not included in the model, as long as the objective of the paper is focused on deriving a reasonable test-case for the modeling technique, rather than exactly reproducing the behavior of the actual vehicle.

A set of pseudo-body axis $\mathcal{F}_B \equiv \{O; x_B, y_B, z_B\}$ is selected [28, 27], which is centered in the centre of mass O of the undeformed configuration, with the

x_B axis parallel to the truss axis, the z_B axis in the symmetry plane, normal to the plane identified by the solar panels, and the y_B axis completing a right-handed triad. Only three deformation degrees of freedom are considered for the truss, namely flexural deformation in the y and z direction, ξ_y and ξ_z, and torsion around the truss axis x_T, parallel to x_B in the undeformed configuration (Figure 1.c).

2.2. FE model of the Truss

A numerical FE model is developed to simulate the structural behavior of the ISS-like truss, in order to numerically obtain the first natural frequencies and relative modal shapes. The commercial software MSC NASTRAN/PATRAN R2019 is used [29].

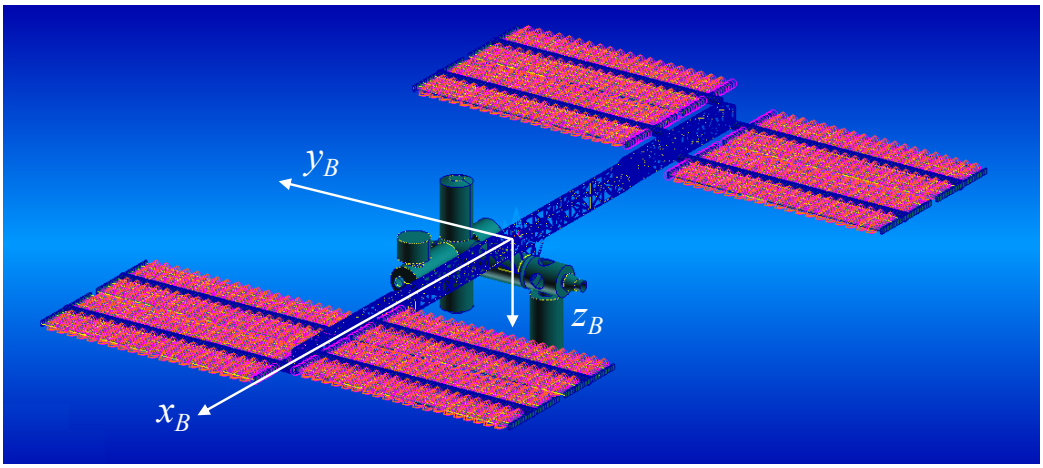

Figure 2: Vehicle FE model.

For sake of clarity, the eight solar panels (magenta rectangles in Figure 2) and the pressurized modules (green cylinders) are drawn, attached at different stations along the flexible truss. The reference frame for structural analysis is centered as indicated in Figure 1.b. The truss structure is modeled by means of CBAR elements, a straight one-dimensional element that connects two grid points, each one with six degrees of freedom. The main features of the CBAR element are the following: (i) this element supports tension and compression, torsion, bending and shear in two perpendicular planes, (ii) the elastic axis and the shear center coincide, (iii) the effect of out-of-plane cross-sectional warping is neglected.

To the best of authors' knowledge, no work is available to the scientific community which analyses in detail the ISS structural behavior. For this reason, the properties of the CBAR elements used in the model (i.e. materials, areas and moments of inertia of each beam element) were empirically derived, based on a few technical data available in the public literature and reasonable assumptions [30, 31, 32].

The FE model thus developed is used to perform modal analyses (SOL103) in order to obtain the first natural frequencies and the first mode shapes, in terms of flexural and torsional degrees of freedom.

2.3. Transport and deformation variables: kinematics

As proposed in [14] and [28], motion variables are divided into transport and deformation degrees of freedom, where the former represent global displacement of the whole vehicle and depend on time only, whereas the latter describe local deformation of the vehicle structure, thus depending on time and position of the mass element along the structure.

In the present case, transport variables are associated to rotational degrees of freedom. The attitude of $\mathcal{F}_B$ with respect to an inertially fixed reference frame $\mathcal{F}_I$ can be described in terms of quaternions $\boldsymbol{Q} = (\boldsymbol{q}^T, \bar{q})^T$, where the vector and scalar parts of the quaternions defined as

$$\boldsymbol{q} = \hat{\boldsymbol{a}} \sin(\alpha/2) \; ; \quad \bar{q} = \cos(\alpha/2)$$

with $\hat{\boldsymbol{a}}$ and α being the unit vector parallel to Euler eigenaxis and Euler rotation angle, respectively, associated to the rotation that takes $\mathcal{F}_B$ onto $\mathcal{F}_I$ [33].

The evolution of quaternions is ruled by

$$\begin{aligned} \dot{\boldsymbol{q}} &= \frac{1}{2}\left(\bar{q}\boldsymbol{\omega} - \boldsymbol{\omega} \times \boldsymbol{q}\right) \\ \dot{\bar{q}} &= -\frac{1}{2}\boldsymbol{\omega}^T \boldsymbol{q} \end{aligned}$$

where $\boldsymbol{\omega}$ are angular velocity components of $\mathcal{F}_B$ with respect to $\mathcal{F}_I$.

In order to derive a finite order system of ordinary differential equations, deformation variables (two flexural DoFs in the xy and xz planes) and a torsional DoF (around x_T) are described using a Galërkin method. Torsion angle $\vartheta(x,t)$ and the flexural displacements $\xi_z(x,t)$, $\xi_y(x,t)$ in the xz and xy

planes, are written as:

$$\begin{aligned}
\vartheta(x,t) &= \sum_{i=1}^{N_t} \psi_i(x) \cdot \zeta_i(t) \\
\xi_z(x,t) &= \sum_{i=1}^{N_f} \phi_i(x) \cdot \eta_{z,i}(t) \\
\xi_y(x,t) &= \sum_{i=1}^{N_f} \phi_i(x) \cdot \eta_{y,i}(t)
\end{aligned}$$

where N_t and N_f are the numbers of relevant assumed modes considered in the analysis, for torsional and flexural DoF's, respectively, $\psi_i(x)$ and $\phi_i(x)$ are the torsional and flexural assumed modes (shape functions) considered, which depend on the position x of the element along the truss axis x_T, and $\zeta_i(t)$, $\eta_{z,i}(t)$, and $\eta_{y,i}(t)$ are time-dependent amplitude of the i–th assumed mode in the discretisation. Deformation rates $\dot{\vartheta}$, $\dot{\xi}_z$, and $\dot{\xi}_y$ are clearly obtained from the same expansion, where the amplitude of the assumed modes is multiplied by $\dot{\zeta}_i$, $\dot{\eta}_{z,i}$, and $\dot{\eta}_{y,i}$, respectively.

As a consequence, the state vector of the whole system can be partitioned as

$$\boldsymbol{x} = (\boldsymbol{\omega}^T, \dot{\boldsymbol{x}}_D^T, \boldsymbol{Q}^T, \boldsymbol{x}_D^T)^T \in \mathbb{R}^N$$

where the vector $\boldsymbol{x}_D = (\zeta_1, \zeta_2, \ldots, \zeta_{N_t}; \eta_{z,1}, \eta_{z,2}, \ldots, \eta_{z,N_f}; \eta_{y,1}, \eta_{y,2}, \ldots, \eta_{y,N_f})^T$ collects deformation states. The order of the system, N, that is, the total number of state variables used for describing the coupled rotational and deformation dynamics of the vehicle, is given by $N = 7 + 2N_t + 4N_f$.

In the following sections, when necessary for the sake of conciseness, variable will be also grouped into position variables, namely $\boldsymbol{P} = (\boldsymbol{Q}^T, \boldsymbol{x}_D^T)^T$, and velocity variables, $\boldsymbol{V} = (\boldsymbol{\omega}^T, \dot{\boldsymbol{x}}_D^T)^T$. Also note that a non-minimal attitude representation is being used, in order to avoid issues with singular attitudes, when Euler angles (such as roll, pitch, and yaw angles) are adopted. Nonetheless, for the sake of clarity, simulation results will be shown in terms of quaternions.

2.4. Equivalent Low-Order Model of the Truss

The most important ingredient of the reduced order model, which allows for representing the main dynamic features of the whole vehicle on the basis of a minimum set of relevant information on structural configuration, is the

definition of structural properties of the deformable element(s). In order to identify these properties, the main truss structure is modeled by means of an Euler-Bernoulli unconstrained beam with constant, thin-walled and hollow section[34].

The aim is to identify the properties of this simplified, constant section beam model, which reproduces with adequate accuracy, the response in the frequency domain of the FE model of the ISS-like truss. Lumped masses and moments of inertia, associated to solar panels and pressurized modules, are than added at different stations along the deformable structure (Figure 3), thus providing a configuration which resembles, at a mass distribution level, that of the actual vehicle.

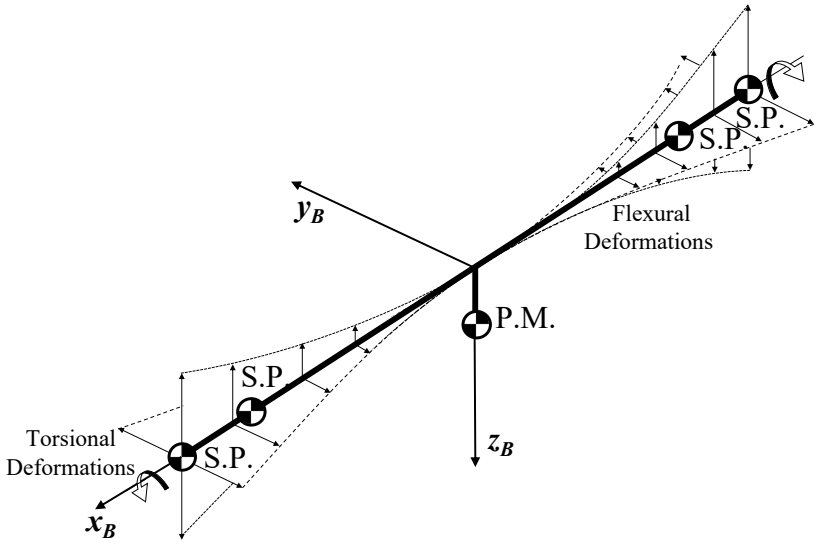

Figure 3: Low-Order Model of the ISS.

The dynamics of torsional angle and flexural displacements of a slender beam with constant section are described by the following equations [35]:

$$\begin{aligned} GI_t \cdot \vartheta^{ii}(x,t) &- J'_x \cdot \ddot{\vartheta}(x,t) = 0 \\ EI_{yy} \cdot \xi_z^{iv}(x,t) &+ m' \cdot \ddot{\xi}_z(x,t) = 0 \\ EI_{zz} \cdot \xi_y^{iv}(x,t) &+ m' \cdot \ddot{\xi}_y(x,t) = 0 \end{aligned}$$

where (i) G and E are shear and flexural moduli, respectively; (ii) I_t, I_{yy} and I_{zz} are the torsional and the second moments of inertia of the section; and

(iii) J'_x and m' are the rotational inertia and mass densities (per unit length) of the truss, respectively, both assumed constant.

By using the Galërkin discretization and the Euler-Bernoulli mode functions (with free-free boundary conditions) as assumed mode shapes, it is possible to evaluate the i_{th} torsional (around x axis) and flexural (in xz and xy planes) natural frequencies

$$f_i^{\vartheta} = \frac{k_i}{2\pi}\sqrt{\frac{GI_t}{\rho I_p}} \quad ; \quad f_i^{xz/xy} = \frac{\beta_i^2}{2\pi}\sqrt{\frac{EI_{yy/zz}}{m/L}}$$

where (i) k_i and β_i are the roots of the characteristic nonlinear equations, depending on boundary conditions; (ii) ρ and m are the material density and the total mass of the truss; and (iii) I_p and L are the polar inertia of the constant section and the truss length, respectively.

Quite obviously, different values of beam section features (I_t/I_p, I_{yy} and I_{zz}) are obtained, for each considered modal frequency. The attention is thus focused on the first two modes, which are assumed as the most relevant ones for the considered coupling problem between deformation and attitude maneuvers (similarly to what was done in [27] and [36] for aeronautical applications of a similar modeling approach). A set of section parameters is thus determined, which minimizes a weighted combinations of the errors between for the first two torsional and flexural natural frequencies derived from the FEM analysis and the low-order model. The validity of this approach will be assessed in Section 4.

3. Reduced-Order Dynamics of a Large Space Structure

3.1. Transport and deformation variables: dynamics

A mixed Newtonian-Lagrangian approach [27] is applied to describe the dynamics of the system using generalized Euler equations for the angular velocities (transport variables) and Lagrange equations of motion for generalized coordinates associated to deformation variables (flexural and torsional variables). Details on the derivation of the full set of equations of motion can be found in [37]. The next two subsections introduce the relevant equations in compact vector form. The definition of vector and matrix quantities is reported in the Appendix.

3.2. Generalized Euler Equation for Attitude Dynamics

When all vector quantities are expressed in the pseudo-body axis reference frame, $\mathcal{F}_B$, generalized Euler equation achieves the form:

$$\frac{d\mathbf{h}}{dt} + \boldsymbol{\omega} \times \boldsymbol{h} + \mathbf{S} \times \mathbf{a}_0 = \mathbf{M} \tag{1}$$

where $\mathbf{h}$ is the angular momentum, $\mathbf{S} = m_{tot}\boldsymbol{r}_{OG}$ is the static moment of the body with respect to the origin O of $\mathcal{F}_B$, $\mathbf{a}_0$ is the acceleration of O, and $\mathbf{M}$ is the total external torque acting on the body. Note that for a purely rotational dynamics, the acceleration of the centre of mass G is zero and

$$\mathbf{a}_0 = -\left(\frac{\mathsf{d}^2\boldsymbol{r}_{OG}}{\mathsf{d}t^2}\right)_I$$

evaluated in an inertial frame. For small deformations, the position of G with respect to O can be expressed as $\boldsymbol{r}_{OG} = \boldsymbol{\Lambda}\boldsymbol{x}_D$.

Letting $\mathbf{J}$ be the moment of inertia tensor, the angular momentum can be expressed as:

$$\mathbf{h} = \underbrace{\mathbf{J}\,\boldsymbol{\omega}}_{\text{rotation term}} + \underbrace{\mathbf{h}_{rel}}_{\text{deformation term}} + \underbrace{\mathbf{H}_B}_{\text{control term}} \tag{2}$$

The rotation term is related to the angular rate of the whole body, where the inertia tensor, $\boldsymbol{J} = \boldsymbol{J}_0 + \Delta\boldsymbol{J}$, is equal to the sum of a nominal value, $\boldsymbol{J}_0$, for the undeformed configuration, plus an increment $\Delta J(\boldsymbol{x}_D)$, due to structure deformation state. The deformation term represents the contribution of deformation rates to angular momentum. For small deformations, it can be written as $\boldsymbol{h}_{rel} = \boldsymbol{\Gamma}\dot{\boldsymbol{x}}_D$. Finally, the control term accounts for the angular momentum of Control Moment Gyroscopes (CMG) used to control the spacecraft. This latter term depends on the orientation of the gimbals, as explained in detail in subsection 3.4.

Expanding and rewriting, the generalized Euler equations can be expressed in the form

$$\left[\boldsymbol{\Gamma} + \Delta\boldsymbol{\Lambda}\right]\,\ddot{\mathbf{x}}_D + \left[\mathbf{J} + \Delta\mathbf{J}_{rcm}\right]\,\dot{\boldsymbol{\omega}} = \mathbf{f}_E(\mathbf{V}, \mathbf{P}) \tag{3}$$

where $\Delta\boldsymbol{\Lambda}\ddot{\mathbf{x}}_D + \Delta\mathbf{J}_{rcm}\dot{\boldsymbol{\omega}}$ accounts for the terms of $\mathbf{S} \times \mathbf{a}_0$ which depend on $\ddot{\mathbf{x}}_D$ and $\dot{\boldsymbol{\omega}}$, whereas $\mathbf{f}_E$ sums up all the contribution which depend on angular rate, deformation and deformation rates, and control terms. For the sake of clarity, all matrices are explicitly defined in the Appendix.

3.3. Lagrange Equations for Dynamics of Deformation variables

Starting from the expressions of kinetic and potential energy of the whole system, T and U, respectively, Lagrange equations of motion for deformation variables collected in the vector $\mathbf{x}_D$ are

$$\frac{d}{dt}\frac{\partial T}{\partial \dot{x}_i} - \frac{\partial T}{\partial x_i} + \frac{\partial U}{\partial x_i} = Q_i \tag{4}$$

The kinetic energy T, of the system is the sum of kinetic energy of each group of component,

$$T = T_{tr} + T_{sp} + T_{pm}$$

namely truss (subscript tr), solar panels (sp), and pressurised modules (pm), whereas potential energy consists only of one term,

$$U = U_{tr} \tag{5}$$

that is, elastic energy related to truss deformation (tr), assuming that, in the absence of external forces, other than gravity, the centre of mass of the system follows its nominal orbit.

3.3.1. Truss

In the simplified scheme, the truss structure is modelled as a constant section slender beam, with constant material and elastic properties. The kinetic energy of a beam element is the sum of a translational and a rotational term,

$$dT_{tr} = \frac{1}{2}\, m'\, V_{tr}^2\, dx_{tr} + \frac{1}{2}\, \boldsymbol{\omega}_P^t\, \mathbf{J}'\, \boldsymbol{\omega}_P\, dx_{tr} \tag{6}$$

where $m' = m_{tr}/L$ is mass per unit length, J'_{xx}, J'_{yy} and J'_{zz} are beam section mass moments of inertia per unit length and $\boldsymbol{\omega}_P$ equal to body plus deformation angular speeds. Integrating over the length L of the truss, the kinetic energy is the sum of a term associated to beam elements velocity, T_V, and a term associated to beam element angular speed, T_ω.

Considering torsional and flexural variables associated to the Galërkin

expansion, one has that

$$\begin{array}{lll}
\dfrac{\partial T_V}{\partial \zeta_i} = 0 & ; & \dfrac{d}{dt}\dfrac{\partial T_V}{\partial \dot{\zeta}_i} = 0 \\
\dfrac{\partial T_V}{\partial \eta_{z,i}} = \text{see [37]} & ; & \dfrac{d}{dt}\dfrac{\partial T_V}{\partial \dot{\eta}_{z,i}} = \text{see [37]} \\
\dfrac{\partial T_V}{\partial \eta_{y,i}} = \text{see [37]} & ; & \dfrac{d}{dt}\dfrac{\partial T_V}{\partial \dot{\eta}_{y,i}} = \text{see [37]} \\
\dfrac{\partial T_\omega}{\partial \zeta_i} = 0 & ; & \dfrac{d}{dt}\dfrac{\partial T_\omega}{\partial \dot{\zeta}_i} = \text{see [37]} \\
\dfrac{\partial T_\omega}{\partial \eta_{z,i}} = 0 & ; & \dfrac{d}{dt}\dfrac{\partial T_\omega}{\partial \dot{\eta}_{z,i}} = \text{see [37]} \\
\dfrac{\partial T_\omega}{\partial \eta_{y,i}} = 0 & ; & \dfrac{d}{dt}\dfrac{\partial T_\omega}{\partial \dot{\eta}_{y,i}} = \text{see [37]}
\end{array}$$

The elastic potential deformation energy of the truss can be written as

$$U_{tr} = \int_{-L/2}^{L/2} \frac{1}{2} G J_t (\theta')^2 dx_{tr} + \int_{-L/2}^{L/2} \frac{1}{2} E I_{yy} (\xi_z'')^2 dx_{tr} + \int_{-L/2}^{L/2} \frac{1}{2} E I_{zz} (\xi_y'')^2 dx_{tr}$$

where E and G are Young module and shear module, whereas J_t, I_{zz}, and I_{yy} are section moments of inertia.

3.3.2. Solar panels

Solar panels are rigidly attached to the truss. Four couples of solar panels are considered. Each couple is considered as a rigid body of equivalent mass and inertia, with the centre of mass on the longitudinal axis of the truss. Note that panels can rotate around a pitch axis, perpendicular to the truss axis.

No potential energy is associated to the panels and only kinetic energy needs to be considered:

$$T_{sp} = \sum_{k=1}^{4} \left(\frac{1}{2} m_{sp,k} V_{sp,k}^2 + \frac{1}{2} \boldsymbol{\omega}_{P,k}^t \, \tilde{\boldsymbol{J}}_{sp,k} \, \boldsymbol{\omega}_{P,k} \right) \tag{7}$$

where $\tilde{\boldsymbol{J}}_{sp}$ is the inertia matrix of the panel pairs in the local reference frame $\mathcal{F}_L$, parallel to $\mathcal{F}_B$, in the undeformed configuration, rigidly connected to the

panel plates, with the origin in the attach point on the truss. In this way, the vibrational behavior of the equivalent truss is significantly influenced by these contributions in Eq. (7) (see Figure 3). At the same time, it is noteworthy to observe that solar panels have mass and inertia of at least two orders of magnitude smaller than the truss to which they are connected. The assumption of rigid solar panels is reasonable, provided that deformation of the panels does not affect significantly the position of the center of mass of the whole system nor its mass distribution in the deformed configuration, making the effect of solar panels deformation on overall large structure dynamic response negligible. On the other hand, such an assumption is useful in simplifying the ISS model in terms of both numbers of generalized coordinates (the description of solar panel deformation would require to add deformation state for all panels) and system parameters (no information on actual stiffness and mass distribution of the solar panes is required, just their inertial parameters).

As for the truss, also for solar panels one has that:

$$\begin{aligned}
&\frac{\partial T_{sp}}{\partial \zeta_i} = 0 \qquad ; \quad \frac{d}{dt}\frac{\partial T_{sp}}{\partial \dot{\zeta}_i} = \text{see [37]} \\
&\frac{\partial T_{sp}}{\partial \eta_{z,i}} = \text{see [37]} \quad ; \quad \frac{d}{dt}\frac{\partial T_{sp}}{\partial \dot{\eta}_{z,i}} = \text{see [37]} \\
&\frac{\partial T_{sp}}{\partial \eta_{y,i}} = \text{see [37]} \quad ; \quad \frac{d}{dt}\frac{\partial T_{sp}}{\partial \dot{\eta}_{y,i}} = \text{see [37]}
\end{aligned}$$

3.3.3. Pressurized modules

Pressurized modules are assumed as a rigid body, attached to the centre of the truss in the undeformed configuration. Consequently, the position of pressurized module assembly is fixed with respect to $\mathcal{F}_B$ and its contribution to total kinetic energy is associated with transport (rotational) degrees of freedom only. This means that the partial derivatives of T_{pm} with respect to deformation DoFs are all zero under the proposed choice of generalized coordinates.

3.3.4. Generalized forces

On the right-hand side of Lagrange equations of motion, the term Q_i contains non-conservative, generalized forces, obtained from the virtual work principle applied to flexible coordinates, $\mathbf{x}_D$,

$$\delta W_i = Q_i \cdot \delta x_i \qquad x_i \in \mathbf{x_D} \tag{8}$$

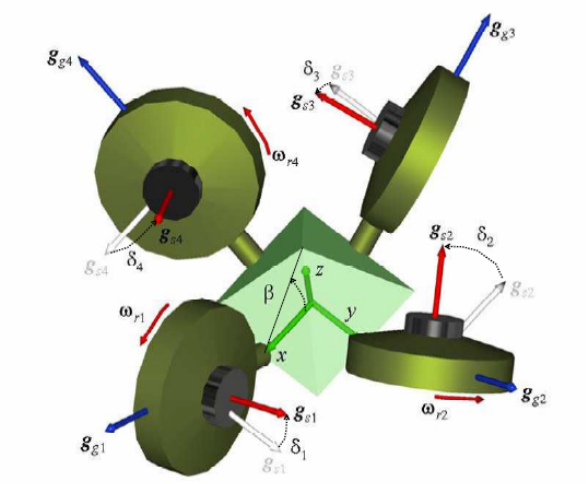

Figure 4: Sketch of the CMG cluster.

where generalised forces are expressed as:

$$\mathbf{Q}_F = \begin{pmatrix} Q_F^{\zeta} \\ Q_F^{\eta_z} \\ Q_F^{\eta_y} \end{pmatrix} \tag{9}$$

3.3.5. Equations for deformation DoF's

In the end, collecting all the terms obtained previously, the resulting system of Lagrange equations can be recast in the form of a set of linear second-order ordinary differential equations,

$$\mathbf{M}\,\ddot{\mathbf{x}}_\mathbf{D} + \mathbf{C}\,\dot{\mathbf{x}}_\mathbf{V} + \mathbf{K}\,\mathbf{x}_\mathbf{D} = \mathbf{Q}_\mathbf{F} + \mathbf{Q}_\mathbf{in} \tag{10}$$

where $\boldsymbol{Q}_{in}$ groups all the inertial contributions from the left-hand side of Lagrange equation. All the matrices are provided in the Appendix. Note that the inertial coupling matrix $\boldsymbol{C}$ depends on the state vector $\boldsymbol{x}$, then it must be evaluated at every time step.

3.4. Control variables

A cluster of control moment gyroscopes is assumed as the effector for 3-axis attitude control [33]. A cluster of 4 CMG's will be considered, in a

pyramid mounting (Figure 4), with a mount angle $\beta = 58$ deg, which results into a quasi-spherical angular momentum envelope. The angular momentum $\boldsymbol{H}$ of the cluster depend on gimbal angles, $\boldsymbol{\delta} = (\delta_1, \delta_2, \delta_3, \delta_4)^T$,

$$\boldsymbol{H} = h_w \begin{pmatrix} -\mathrm{c}\beta\mathrm{s}\delta_1 - \mathrm{c}\delta_2 + \mathrm{c}\beta\mathrm{s}\delta_3 + \mathrm{c}\delta_4 \\ \mathrm{c}\delta_1 - \mathrm{c}\beta\mathrm{s}\delta_2 - \mathrm{c}\delta_3 + \mathrm{c}\beta\mathrm{s}\delta_4 \\ \mathrm{s}\beta\mathrm{s}\delta_1 + \mathrm{s}\beta\mathrm{s}\delta_2 + \mathrm{s}\beta\mathrm{s}\delta_3 + \mathrm{s}\beta\mathrm{s}\delta_4 \end{pmatrix}$$

where $\mathrm{s}(\cdot) = \sin(\cdot)$ and $\mathrm{c}(\cdot) = \cos(\cdot)$, and h_w is the angular momentum stored in each cluster wheel, assumed constant (variable speed CMG's will not be considered in the present applications).

The apparent gyroscopic torque obtained from the CMG cluster is equal to

$$\boldsymbol{m}_g = -\dot{\boldsymbol{H}} - \boldsymbol{\omega} \times \boldsymbol{H}$$

where $\dot{\boldsymbol{H}} = \boldsymbol{A}(\delta)\dot{\boldsymbol{\delta}}$, and $\boldsymbol{A} = \partial \boldsymbol{H}/\partial \boldsymbol{\delta}$ is a Jacobian matrix (see Appendix).

The control vector is thus given by gimbal rates, $\boldsymbol{u} = \dot{\boldsymbol{\delta}}$, which can be determined in order to provide a desired control torque, derive from other control approaches, such as the quaternion feedback control law [33]. A wide literature on singularity avoidance [38] and singularity robust [39] techniques is available, in order to allow the command law to either circumvent or cross cluster singular configurations. A singularity avoidance gimbal rate command low is here adopted (see Appendix).

3.5. System dynamic model

The models developed in the previous subsections can be assembled into a system of first-order ordinary differential equations in the time domain, Recalling that the vector $\mathbf{V}$ groups velocities variables (angular rates and assumed mode rates), whereas $\mathbf{P}$ lists position variables (quaternion and assumed modes amplitudes), an explicit space-state formulation can be derived,

$$\dot{\mathbf{V}} = [\mathbf{M}^*]^{-1}\mathbf{f}(\mathbf{V}, \mathbf{P}) \tag{11}$$

$$\dot{\mathbf{P}} = \begin{pmatrix} -\frac{1}{2}\,\boldsymbol{\omega}^T\,\mathbf{q} \\ \frac{1}{2}(q_0\boldsymbol{\omega} - \boldsymbol{\omega} \times \mathbf{q}) \\ \dot{\mathbf{x}}_\mathbf{D} \end{pmatrix} = \mathbf{g}(\mathbf{V}, \mathbf{P}) \tag{12}$$

where the mass matrix $\mathbf{M}^*$ is defined as

$$\mathbf{M}^* = \begin{bmatrix} \mathbf{J} + \Delta\mathbf{J}_{rcm} & \boldsymbol{\Gamma} + \boldsymbol{\Delta\Lambda}] \\ \mathbf{C} & \mathbf{M} \end{bmatrix}$$

The system formed by Eqs. (11) and (12) can be solved numerically, by means of a step integration algorithm.

Table 1: Beam section features and natural frequencies.

Beam Section	[Hz]	FEM	L – O	Err [%]
I_t/I_p=0.0217	f_1^ϑ	2.12	2.26	6.60
	f_2^ϑ	7.29	6.67	-8.50
I_{yy}=0.0084 [m^4]	f_1^{xz}	1.17	1.08	-7.69
	f_2^{xz}	2.65	2.80	5.66
I_{zz}=0.0035 [m^4]	f_1^{xy}	0.73	0.68	-6.85
	f_2^{xy}	1.87	1.76	-5.88

4. Results

4.1. Free dynamics of the (equivalent) truss

By following the approach proposed in Subsec. 2.4, a minimum for the weighted combination of the errors on the estimate of the first two frequencies for torsional and flexural modes derived from the FE model and the equivalent Euler-Bernouilli beam is determined. The corresponding results are provided in Table 1), where the features of the thin-walled hollow section are also reported. The overall correlation between the estimate of the actual frequencies and those derived for the semi-analytical equivalent beam appears satisfactory, thus offering a promising tool for the analysis of coupling between vehicle attitude manoeuvre and truss deformation. The main reason of the errors provided in Table 1 lies in the features of the different truss models, when use is made of a Finite Element (FE) approach or a Low-Order (L-O) model. The ISS-like truss in Figure 2 is modelled with CBAR elements, while the equivalent Euler-Bernouilli beam in Figure 3 is assumed having a uniform thin-wall and hollow section. The modal behavior of the truss is influenced by the distribution of mass and stiffness, along the main axis, coming from the complex assembly of bars, while the homogenous slender beam is characterized by a uniform density and cross sectional area. The difference in terms of natural frequencies is the unavoidable price to pay for having a reduced order model and this, indeed, limits its use to preliminary design evaluations.

The modal shape functions of the equivalent Euler-Bernouilli beam are then used as the assumed modes for modelling the dynamic behaviour of the whole vehicle, featuring all the additional elements (solar panels and pressurised modules), following the procedure outlined in Section 3.

Prior to this step, some simulations are shown which demonstrate the validity of the results derived for modelling the equivalent beam withe the assumed modes method, including the rotational inertia of the beam section, which is not included in the elementary Euler-Bernouilli beam adopted for enforcing the value of the frequency derived from the FE model.

A non-zero initial condition is thus provided to each Galërkin expansion variable. The natural frequencies of the free truss (*i.e.* the system without solar panels and pressurised modules) are thus obtained from the simulation and compared to the ones shown in the Table 1.

For $\zeta_1(\mathbf{x}, t = 0) = 0.1$ and $\zeta_2(\mathbf{x}, t = 0) = 0.1$ torsional modes are excited. The response for these two cases is shown in Fig 5. As expected, torsional modes are decoupled and no angular velocity component (not reported) arise. The natural frequencies found are close to the FEM ones, with an error smaller than 10%.

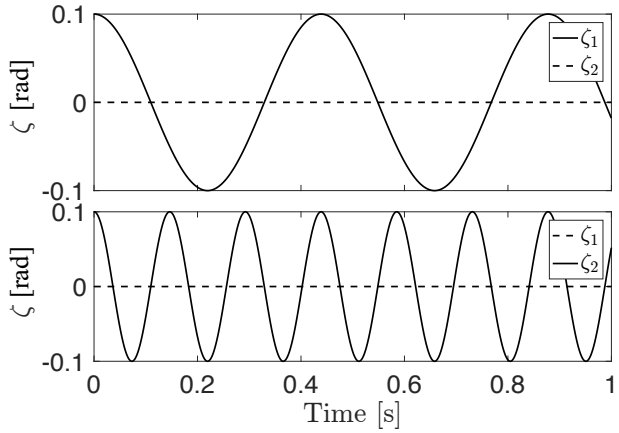

Figure 5: First and second torsional mode dynamics

The results for deformation in the x-z plane are addressed in Figure 6, where deformation variables $\eta_{z,1}(\mathbf{x}, t = 0) = 0.1$ (with $\eta_{z,2} = 0$) and $\eta_{z,2}(\mathbf{x}, t = 0) = 0.1$ (with $\eta_{z,1} = 0$) are used as initial conditions for the two numerical simulation. Once again, the responses exhibits a negligible coupling, with a negligible excitation of pitch angular velocity component, ω_2 arising in the second case, provided the second mode is characterised by an antisymmetric shape function. Provided the values of ω_2 remain below 10^{-6} rad/s, the effect is assumed negligible and not shown in the figures.

A similar result is obtained for flexural deformation in the x-y plane, when $\eta_{y,1}(\mathbf{x}, t = 0) = 0.1$ (with $\eta_{y,2} = 0$) and $\eta_{y,2}(\mathbf{x}, t = 0) = 0.1$ (with

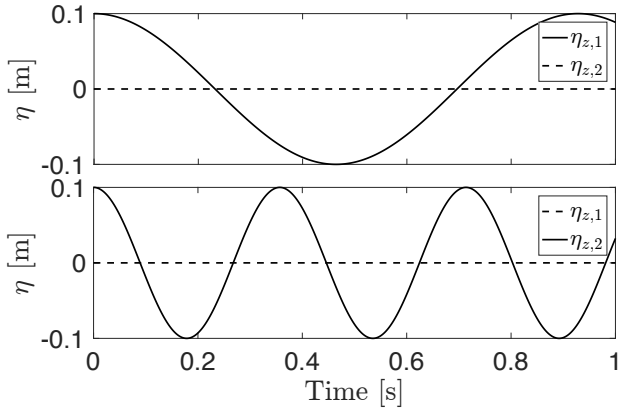

Figure 6: First and second flexural mode in xz plane

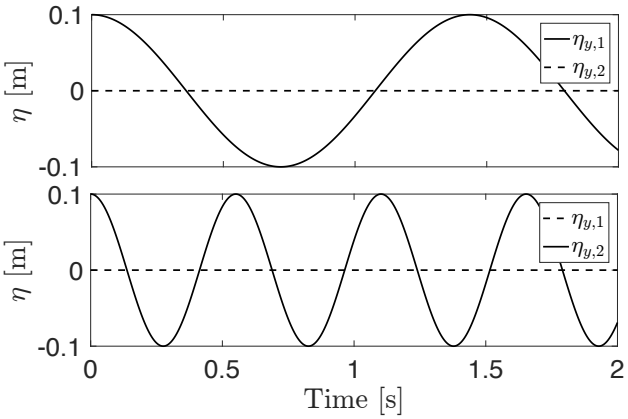

Figure 7: First and second flexural mode in xy plane

(with $\eta_{y,1} = 0$). As for the x-z plane, a negligible coupling between first and second modes occurs (Figure 7), and ω_3 is again only marginally influenced by the second antisymmetric mode. In both cases, the natural frequencies are comparable with the FEM model ones, with a relative error smaller than 10%.

4.2. Open-loop control

As a first example of forced behavior of the whole vehicle, an open-loop control law is discussed, based on a doublet command input on gimbal rates for CMG 1 and 3, providing an apparent gyroscopic torque command around x-axis. Figure 8.a shows the gimbal rate command $\dot{\delta}_\star$ and the resulting gimbal angle $\delta_\star$, with $\delta_1 = \delta_\star$ and $\delta_3 = -\delta_\star$.

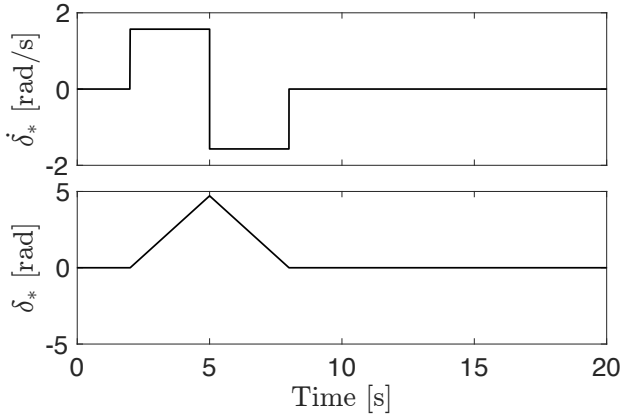

Figure 8: Doublet command.

The system responds with a rotation around the x axis. Coupling with deformation in the x-z and x- y planes is induced by pressurized module inertia during the rotation. The variation of angular velocity components of $\mathcal{F}_B$ (top subplot) is clearly dominated by ω_1, for the considered control input, with a resulting variation of the first component of the quaternion vector, q_1 (central subplot). The apparent gyroscopic torque, reported in the subplot at the bottom of Figure 9, exhibit a step variation of the command torque at maneuver start ($t_0 = 2$ s) and maneuver end ($t_1 = 7$ s).

It is worthwhile observing in Figure 8.b the zero torque line: ω_1 decreases before the zero torque time, because of the torsional reaction of the truss. A persistent oscillation of roll rate ω_1 and quaternion component q_1 is evident,

for $t > t_1$ (no structural damping is modeled at present), which is caused by the torsional spring effect of the truss, under the action of inertial loads of solar panels, placed close to the free end of the truss and those of the group of pressurized modules, placed at its centre. The value of q_1 oscillates around a non-zero mean value, with oscillation amplitude wider than the average value. Clearly, a sharp control torque profile like that depicted in the bottom subplot is the main cause of such an undesired behaviour, which would lead to pointing errors of all pieces of equipment placed along the truss.

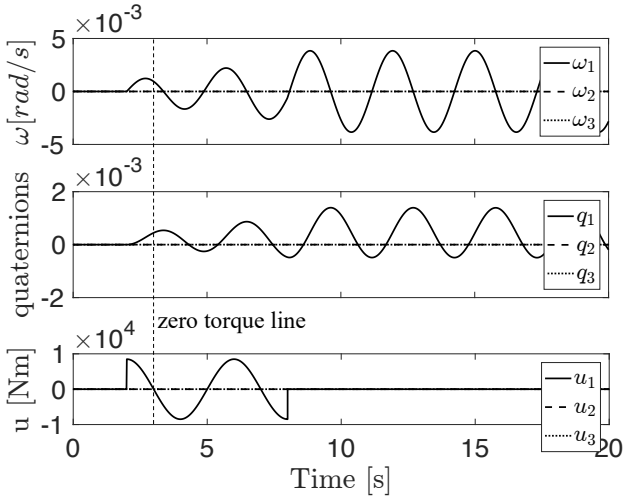

Figure 9: Response to a gyroscopic torque command around x.

4.3. Closed-loop feedback control

A second maneuver is now considered, under the action of a Quaternion-Feedback Control (QFC) law, coupled with a gimbal rate command based on Moore-Penrose pseudo-inverse and null motion for singularity avoidance (see Appendix for details).

A non-zero initial value for q_1 is assumed, which corresponds to an angular error of 5 deg around the x-axis. Figure 10 demonstrates how the gimbal rate command drives the spacecraft towards the prescribed attitude in approximately 60 s, with relevant oscillations of all attitude variables during the maneuver. Figure 11 provides the response of modal amplitudes, excited by the initial step variation of the apparent control torque. After the end

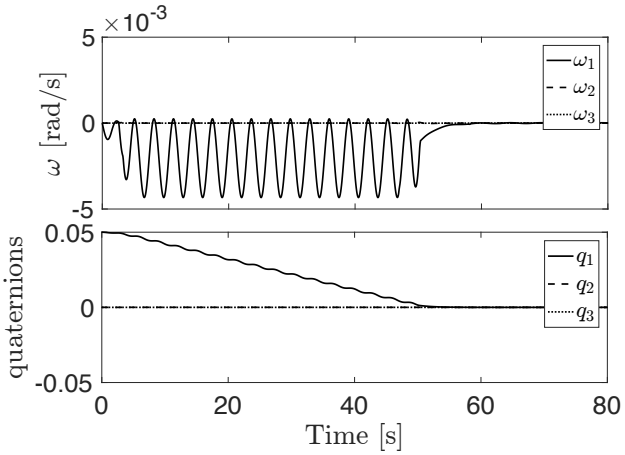

Figure 10: QFC response for an error on q_1.

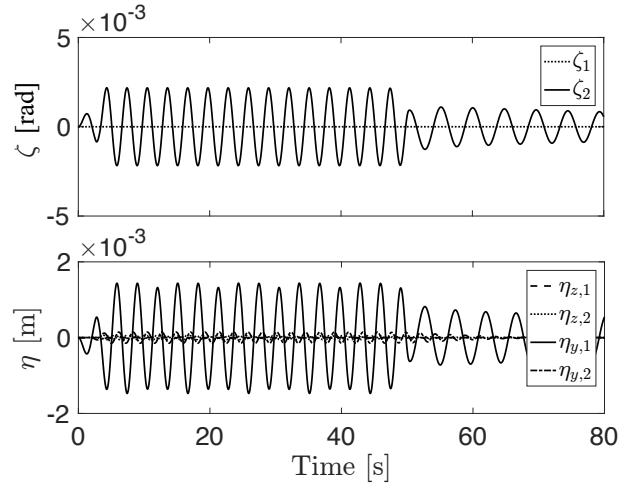

Figure 11: Structural excitation during QFC response.

of the maneuver, persistent torsional and flexural vibrations are present, although with a reduced amplitude. Clearly, a smooth command law should be envisaged, which limits the initial excitation during the acceleration phase, at maneuver start.

5. Conclusions

A modeling technique is proposed, which allows to derive low-order models of large deformable space structures, for the analysis of coupling phenomena between attitude maneuvers and structure deformation. The approach is based on the identification of a simplified equivalent Euler-Bernouilli beam, which reproduces the main elastic features of the actual truss structure. Then a hybrid Newtonian-Lagrangian approach is adopted for deriving the model of the whole vehicles, which includes additional elements, modeled as rigid bodies attached along the truss. The formulation of vehicle dynamics is reported and described and some open-loop and closed-loop maneuver examples are reported, when a cluster of control moment gyroscopes is adopted as attitude effectors. The numerical simulations allowed for an insight on the tight coupling between apparent gyroscopic control torque and the resulting vibration induced during the maneuver.

Appendix

Terms of generalized Euler equation for $\boldsymbol{\omega}$

Under the hypothesis of small deformations, the displacement of the centre of mass with respect to the origin of $\mathcal{F}_B$ and the angular momentum provided by deformation rates are given by $\boldsymbol{r}_{OG} = \boldsymbol{\Lambda}\boldsymbol{x}_D$ and $\boldsymbol{h}_{rel} = \boldsymbol{\Gamma}\dot{\boldsymbol{x}}_D$, respectively, with

$$\boldsymbol{\Lambda} = \begin{bmatrix} [0]_{1\times N_t} & [0]_{1\times N_f} & [0]_{1\times N_f} \\ [0]_{1\times N_t} & [0]_{1\times N_f} & \boldsymbol{\Lambda}^y \\ [0]_{1\times N_t} & \boldsymbol{\Lambda}^z & [0]_{1\times N_f} \end{bmatrix}$$

$$\boldsymbol{\Gamma} = \begin{bmatrix} \boldsymbol{\Gamma}_{tors} & [0]_{1\times N_f} & \boldsymbol{\Gamma}_{xy} \\ [0]_{1\times N_t} & \boldsymbol{\Gamma}^y_{flex} & [0]_{1\times N_f} \\ [0]_{1\times N_t} & [0]_{1\times N_f} & \boldsymbol{\Gamma}^z_{flex} \end{bmatrix}$$

where:

$$\Lambda^y_i = \Lambda^z_i = \frac{1}{m_{tot}}[\int_{-L/2}^{L/2} \phi_i dx_{tr} + \sum_{k=1}^{4} m_{sp}\phi_i(x_{sp,k})]$$

for $i = 1, 2 \ldots N_f$;

$$(\Gamma_{tors})_i = J'_x \int_{-L/2}^{L/2} \psi_i dx_{tr} + \sum_{k=1}^{4} J_{sp,1} \psi_i(x_{sp,k})$$

for $i = 1, 2 \ldots N_t$;

$$(\Gamma_{xy})_i = m' d_{tr} \int_{-L/2}^{L/2} \phi_i dx_{tr} + \sum_{k=1}^{4} m_{sp,k}\, d_{tr}\, \phi_i(x_{sp,k})$$

$$(\Gamma^y_{flex})_i = -m' \int_{-L/2}^{L/2} \phi_i x_{tr} dx_{tr} - J'_y \int_{-L/2}^{L/2} \phi'_i dx_{tr} +$$

$$+ \sum_{k=1}^{4} [-m_{sp} x_{sp,k} \phi_i(x_{sp,k}) - J_{sp,2} \phi'_i(x_{sp,k})]$$

$$(\Gamma^z_{flex})_i = m' \int_{-L/2}^{L/2} \phi_i x_{tr} dx_{tr} + J'_z \int_{-L/2}^{L/2} \phi'_i dx_{tr} +$$

$$+ \sum_{k=1}^{4} [m_{sp} x_{sp,k} \phi_i(x_{sp,k}) + J_{sp,2} \phi'_i(x_{sp,k})]$$

for $i = 1, 2 \ldots N_f$.

The acceleration $\mathbf{a}_0$, expressed in terms of pseudo-body frame components, is given by

$$\mathbf{a}_0 = -\ddot{\boldsymbol{r}}_{OG} - \dot{\boldsymbol{\omega}} \times \boldsymbol{r}_{OG} - 2\boldsymbol{\omega} \times \dot{\boldsymbol{r}}_{OG} - \boldsymbol{\omega} \times \boldsymbol{\omega} \times \boldsymbol{r}_{OG}$$

And the static moment term is

$$\mathbf{S} \times \mathbf{a}_0 = m_{tot} \boldsymbol{r}_{0G} \times \mathbf{a}_0$$

Upon substitution of $\boldsymbol{r}_{OG} = \boldsymbol{\Lambda} \boldsymbol{x}_D$, $\dot{\boldsymbol{r}}_{OG} = \boldsymbol{\Lambda} \dot{\boldsymbol{x}}_D$, and $\ddot{\boldsymbol{r}}_{OG} = \boldsymbol{\Lambda} \ddot{\boldsymbol{x}}_D$, one can derive the expressions for matrices $\Delta\boldsymbol{\Lambda}$ and $\boldsymbol{J}_{rmc}$. In particular

$$\Delta\boldsymbol{\Lambda} = m_{tot} \begin{bmatrix} [0]_{1\times N_t} & -y_G \boldsymbol{\Lambda}^y & z_G \boldsymbol{\Lambda}^z \\ [0]_{1\times N_t} & [0]_{1\times N_f} & [0]_{1\times N_f} \\ [0]_{1\times N_t} & [0]_{1\times N_f} & [0]_{1\times N_f} \end{bmatrix}$$

$$\Delta\boldsymbol{J}_{rcm} = -m_{tot} \begin{bmatrix} (y_G^2 + z_G^2) & 0 & 0 \\ 0 & z_G^2 & -y_G z_G \\ 0 & -y_G z_G & y_G^2 \end{bmatrix}$$

Terms of Lagrange equation for deformation variables

Mass Matrix

$$\boldsymbol{M} = \begin{bmatrix} \boldsymbol{M_{\zeta\zeta}} & [0]_{N_f \times N_f} & \mathbf{M}_{\zeta\eta_{\boldsymbol{y}}} \\ [0]_{N_f \times N_t} & \boldsymbol{M_{\eta_z \eta_z}} & [0]_{N_f \times N_f} \\ \mathbf{M}_{\eta_{\boldsymbol{y}}\zeta} & [0]_{N_f \times N_f} & \boldsymbol{M_{\eta_y \eta_y}} \end{bmatrix}$$

with

$$(M_{\zeta\zeta})_{i,j} = J'_x \int_{-L/2}^{L/2} \psi_i \psi_j dx_{tr} +$$

$$+ \sum_{k=1}^{4} \tilde{J}_{sp,1}\, \psi_i(x_{sp,k}) \psi_j(x_{sp,k})$$

for $i, j = 1, 2 \ldots N_t$

$$(M_{\eta_z \eta_z})_{i,j} = m' \int_{-L/2}^{L/2} \phi_i \phi_j dx_{tr} + J'_y \int_{-L/2}^{L/2} \phi'_i \phi'_j dx_{tr} +$$

$$+ \sum_{k=1}^{4} [m_{sp} \phi_i(x_{sp,k}) \phi_j(x_{sp,k}) + \tilde{J}_{sp,2} \phi'_i(x_{sp,k}) \phi'_j(x_{sp,k})]$$

$$(M_{\eta_y \eta_y})_{i,j} = m' \int_{-L/2}^{L/2} \phi_i \phi_j dx_{tr} + J'_z \int_{-L/2}^{L/2} \phi'_i \phi'_j dx_{tr} +$$

$$+ \sum_{k=1}^{4} [m_{sp} \phi_i(x_{sp,k}) \phi_j(x_{sp,k}) + \tilde{J}_{sp,3}\, \phi'_i(x_{sp,k}) \phi'_j(x_{sp,k})]$$

for $i, j = 1, 2 \ldots N_f$

$$(M_{\zeta\eta_y})_{i,j} = (M_{\eta_y \zeta})_{j,i} = \sum_{k=1}^{4} -\tilde{J}_{sp,13}\, \phi'_j(x_{sp,k}) \psi_i(x_{sp,k})$$

for $i = 1, 2 \ldots N_t$ and $j = 1, 2 \ldots N_f$

Stiffness Matrix

$$\mathbf{K} = \begin{bmatrix} \boldsymbol{K_{\zeta\zeta}} & [0]_{N_f \times N_f} & [0]_{N_f \times N_f} \\ [0]_{N_f \times N_t} & \boldsymbol{K_{\eta_z \eta_z}} & [0]_{N_f \times N_f} \\ [0]_{N_f \times N_t} & [0]_{N_f \times N_f} & \boldsymbol{K_{\eta_y \eta_y}} \end{bmatrix}$$

with

$$(K_{\zeta\zeta})_{i,j} = GJ_t \int_{-L/2}^{L/2} \psi_i' \psi_j' dx_{tr}$$

for $i, j = 1, 2 \ldots N_t$

$$(K_{\eta_z\eta_z})_{i,j} = EI_{yy} \int_{-L/2}^{L/2} \phi_i'' \phi_j'' dx_{tr}$$

$$(K_{\eta_y\eta_y})_{i,j} = EI_{zz} \int_{-L/2}^{L/2} \phi_i'' \phi_j'' dx_{tr}$$

for $i, j = 1, 2 \ldots N_f$

Inertial Coupling Matrix

$$\mathbf{C} = \begin{bmatrix} \mathbf{C_{11}} & [0]_{N_t \times 1} & \mathbf{C_{31}} \\ \mathbf{C_{12}} & \mathbf{C_{22}} & [0]_{N_f \times 1} \\ \mathbf{C_{13}} & [0]_{N_f \times 1} & \mathbf{C_{33}} \end{bmatrix}$$

with

$$(C_{11})_i = J_x' \int_{-L/2}^{L/2} \psi_i dx_{tr} + \sum_{k=1}^{4} [\tilde{J}_{sp,1} \psi_i(x_{sp,k})]$$

$$(C_{31})_i = \sum_{k=1}^{4} -\tilde{J}_{sp,13}\, \psi_i(x_{sp,k})$$

for $i = 1, 2 \ldots N_t$

$$(C_{12})_i = m' \sum_{j=1}^{N_f} [(\int_{-L/2}^{L/2} \phi_i \phi_j dx_{tr}) \eta_{y,j}] +$$

$$+ \sum_{k=1}^{4} [m_{sp} \sum_{j=1}^{N_f} \phi_i(x_{sp,k}) \phi_j(x_{sp,k}) \eta_{y,j}]$$

$$(C_{22})_i = -m' \int_{-L/2}^{L/2} \phi_i x_{tr} dx_{tr} - J_y' \int_{-L/2}^{L/2} \phi_i' dx_{tr} +$$

$$+ \sum_{k=1}^{4} [-m_{sp} x_{sp,k} \phi_i(x_{sp,k}) - J_{sp,2} \phi_i'(x_{sp,k})]$$

$$(C_{13})_i = m' d_{tr} \int_{-L/2}^{L/2} \phi_i dx_{tr} - m' \sum_{j=1}^{N_f} (\int_{-L/2}^{L/2} \phi_j \phi_i dx_{tr}) \eta_{z,j} +$$

$$+ \sum_{k=1}^{4} [m_{sp} d_{tr} \phi_i(x_{sp,k}) - m_{sp} \sum_{j=1}^{N_f} (\phi_i(x_{sp,k}) \phi_j(x_{sp,k}) \eta_{z,j}) +$$

$$- \tilde{J}_{sp,1}\, \phi_i'(x_{sp,k})]$$

$$(C_{33})_i = m' \int_{-L/2}^{L/2} \phi_i x_{tr} dx_{tr} + J_z' \int_{-L/2}^{L/2} \phi_i' dx_{tr} +$$

$$+ \sum_{k=1}^{4} [m_{sp} x_{sp,k} \phi_i(x_{sp,k}) + \tilde{J}_{sp,3} \phi_i'(x_{sp,k})]$$

for $i = 1, 2 \ldots N_f$.

Inertial terms in the generalized force vector

$$\mathbf{Q}_{in} = \begin{pmatrix} (0)_{N_t} \\ Q_{in}^{\eta_z} \\ Q_{in}^{\eta_y} \end{pmatrix}$$

with

$$(Q_{in}^{\eta_z})_i = -m' \omega_1 \sum_{j=1}^{N_f} (\int_{-L/2}^{L/2} \phi_i \phi_j dx_{tr}) \dot{\eta}_{y,j} + \frac{\partial T_V}{\partial \eta_{z,i}}$$

$$-(m_{sp} \sum_{j=1}^{N_f} \phi_j(x_{sp,k}) \phi_i(x_{sp,k}) \dot{\eta}_{y,j}) \omega_1 + \frac{\partial T_{sp}}{\partial \eta_{z,i}}$$

$$(Q_{in}^{\eta_y})_i = -m' \omega_1 \sum_{j=1}^{N_f} (\int_{-L/2}^{L/2} \phi_i \phi_j dx_{tr}) \dot{\eta}_{z,j} + \frac{\partial T_V}{\partial \eta_{y,i}}$$

$$-(m_{sp} \sum_{j=1}^{N_f} \phi_j(x_{sp,k}) \phi_i(x_{sp,k}) \dot{\eta}_{y,j}) \omega_1 + \frac{\partial T_{sp}}{\partial \eta_{y,i}}$$

Solar panels inertia

In the previous equations the position of solar panels along the truss is $\mathbf{x}_P = (x_{sp,1}\, x_{sp,2}\, x_{sp,3}\, x_{sp,4})^t$ and the matrix of inertia of each panel $\tilde{\boldsymbol{J}}_{sp}$ in the local frame is

$$\tilde{J}_{sp} = \begin{bmatrix} \tilde{J}_{sp,1} & 0 & \tilde{J}_{sp,13} \\ 0 & \tilde{J}_{sp,2} & 0 \\ \tilde{J}_{sp,31} & 0 & \tilde{J}_{sp,3} \end{bmatrix}$$

with

$$\begin{aligned} \tilde{J}_{sp,1} &= J_{sp,1}\cos^2\theta_{sp} + J_{sp,3}\sin^2\theta sp \\ \tilde{J}_{sp,13} &= \tilde{J}_{sp,31} = (J_{sp,3} - J_{sp,1})\sin\theta sp\cos\theta sp \\ \tilde{J}_{sp,2} &= J_{sp,2} \\ \tilde{J}_{sp,3} &= J_{sp,3}\cos^2\theta sp + J_{sp,1}\sin^2\theta sp \\ \theta sp &= (\theta_1\,\theta_2\,\theta_3\,\theta_4)^t \quad \text{panels pitch angles} \end{aligned}$$

where $J_{p,1}$, $J_{p,2}$, and $J_{p,3}$ and solar panels principal moments of inertia.

Gimbal command

For a desired control torque, $\boldsymbol{m}_c$, the Jacobian matrix

$$\boldsymbol{A} = h_w \begin{bmatrix} -\mathrm{c}\beta\mathrm{c}\delta_1 & \mathrm{s}\delta_2 & \mathrm{c}\beta\mathrm{c}\delta_3 & -\mathrm{s}\delta_4 \\ -\mathrm{s}\delta_1 & -\mathrm{c}\beta\mathrm{c}\delta_2 & \mathrm{s}\delta_3 & \mathrm{c}\beta\mathrm{c}\delta_4 \\ \mathrm{s}\beta\mathrm{c}\delta_1 & \mathrm{s}\beta\mathrm{c}\delta_2 & \mathrm{s}\beta\mathrm{c}\delta_4 & \mathrm{s}\beta\mathrm{c}\delta_4 \end{bmatrix} \in \mathbb{R}^{3\times 4}$$

determines the angular momentum rate command,

$$\dot{\boldsymbol{H}}_c = \boldsymbol{A}\dot{\boldsymbol{\delta}} = -\boldsymbol{m}_c - \boldsymbol{\omega}\times\boldsymbol{H}$$

A gimbal rate command is obtained in the form

$$\dot{\boldsymbol{\delta}} = -\boldsymbol{A}^{\#}\dot{\boldsymbol{H}}_c - \gamma\hat{\boldsymbol{n}}$$

where $\boldsymbol{A}^{\#} = \boldsymbol{A}^T\left(\boldsymbol{A}\boldsymbol{A}^T\right)^{-1}$ is the Moore–Pensose (MP) pseudoinverse matrix, whereas $\hat{\boldsymbol{n}}$ is the direction of the null space of $\boldsymbol{A}$. The MP pseudo-inverse provides the minimum norm solution to the redundant problem $\boldsymbol{A}\boldsymbol{x} = \boldsymbol{b}$, with $\boldsymbol{x}\in\mathbb{R}^n$, $\boldsymbol{x}\in\mathbb{R}^m$, for $n > m$. The term $\gamma\hat{\boldsymbol{n}}$, referred to as null motion, provides a gimbal rate command which does not add anything to the resulting apparent torque, but allows for singularity avoidance. The weight γ is zero,

if the singularity measure $m = \sqrt{\det\left(\boldsymbol{A}\boldsymbol{A}^T\right)}$ is sufficiently far from 0, and it is increased when a singularity is approached, in order to maintain the cluster far from it.

The desired control torque

$$\boldsymbol{m}_c = -\boldsymbol{K}_P\boldsymbol{q} - \boldsymbol{K}_D\boldsymbol{\omega}$$

is derived according to the quaternion-feedback control law [33]. Simple diagonal matrices $\boldsymbol{K}_P$ and $\boldsymbol{K}_D$ can be adopted, with gains determined from requirements on bandwidth and damping similar to those adopted in standard proportional-derivative feedback laws.

References

[1] K. Alipour, P. Zarafshan, A. Ebrahimi, Dynamics modeling and attitude control of a flexible space system with active stabilizers, Nonlinear Dynamics 84 (4) (2016) 2535–2545. https://doi.org/10.1007/s11071-016-2663-y.

[2] P. W. Likins, Dynamics and control of flexible space vehicles, Tech. rep. (1970).

[3] Y. Zhu, L. Guo, J. Qiao, W. Li, An enhanced anti-disturbance attitude control law for flexible spacecrafts subject to multiple disturbances, Control Engineering Practice 84 (2019) 274–283. https://doi.org/10.1016/j.conengprac.2018.11.001.

[4] R. Malla, C. Lin, Dynamics of flexible structures in orbit under jet impingement loading, in: 43rd AIAA/ASME/ASCE/AHS/ASC Structures, Structural Dynamics, and Materials Conference, 2002, p. 1507. https://doi.org/10.2514/6.2002-1507.

[5] A. García-Pérez, Á. Sanz-Andrés, G. Alonso, M. C. Manguán, Dynamic coupling on the design of space structures, Aerospace Science and Technology 84 (2019) 1035–1048. https://doi.org/10.1016/j.ast.2018.11.045.

[6] F. Angeletti, P. Iannelli, P. Gasbarri, M. Sabatini, End-to-end design of a robust attitude control and vibration suppression system for large space smart structures, Acta Astronautica 187 (2021) 416–428. https://doi.org/10.1016/j.actaastro.2021.04.007.

[7] F. Angeletti, P. Gasbarri, M. Sabatini, P. Iannelli, Design and performance assessment of a distributed vibration suppression system of a large flexible antenna during attitude manoeuvres, Acta Astronautica 176 (2020) 542–557. https://doi.org/10.1016/j.actaastro.2020.04.015.

[8] C.-S. Oh, H. Bang, Deployable space structure control using adaptive predictive controller with notch filter, Aerospace Science and Technology 13 (8) (2009) 459–465. https://doi.org/10.1016/j.ast.2009.07.001.

[9] L. Tang, Z. Guo, X. Guan, Y. Wang, K. Zhang, Integrated control method for spacecraft considering the flexibility of the spacecraft bus, Acta Astronautica 167 (2020) 73–84. https://doi.org/10.1016/j.actaastro.2019.08.030.

[10] D. J. Lucia, P. S. Beran, W. A. Silva, Reduced-order modeling: new approaches for computational physics, Progress in aerospace sciences 40 (1-2) (2004) 51–117. https://doi.org/10.1016/j.paerosci.2003.12.001.

[11] J. L. Junkins, Y. Kim, Introduction to dynamics and control of flexible structures: American institute of aeronautics and astronautics, Inc., Washington, DC (1993) 25–27https://doi.org/10.2514/4.862076.

[12] L. Zhu, J. Guo, E. Gill, Review of reaction spheres for spacecraft attitude control, Progress in Aerospace Sciences 91 (2017) 67–86. https://doi.org/10.1016/j.paerosci.2017.04.001.

[13] L. Feng, Y. Baozeng, A. K. Banerjee, T. Yong, W. Wenjun, L. Zhengyong, Large motion dynamics of in-orbit flexible spacecraft with large-amplitude propellant slosh, Journal of Guidance, Control, and Dynamics 43 (3) (2020) 438–450. https://doi.org/10.2514/1.G004685.

[14] L. Meirovitch, Hybrid state equations of motion for flexible bodies in terms of quasi-coordinates, Journal of Guidance, Control, and Dynamics 14 (5) (1991) 1008–1013. https://doi.org/10.2514/3.20743.

[15] M. Chiba, H. Magata, Coupled pitching dynamics of flexible space structures with on-board liquid sloshing, Acta Astronautica 181 (2021) 151–166. https://doi.org/10.1016/j.actaastro.2020.11.002.

[16] B. Thao, The international space station: Three dimensional computer model where technologies of multi-body dynamics, finite element modeling, and control system design meet iss mission 1j shuttle mission sts-126, Ph.D. thesis, California State University, Sacramento (2008).

[17] M. Karpenko, S. Bhatt, N. Bedrossian, A. Fleming, I. M. Ross, First flight results on time-optimal spacecraft slews, Journal of Guidance, Control, and Dynamics 35 (2) (2012) 367–376. https://doi.org/10.2514/1.54937.

[18] J. Guo, C. J. Damaren, Y. Geng, Space structure vibration suppression using control moment gyroscope null motion, Journal of Guidance, Control, and Dynamics 42 (10) (2019) 2272–2278. https://doi.org/10.2514/1.G004344.

[19] G. Margulies, Geometric theory of single-gimbal control moment gyro system, J. Astronaut. Sci. 26 (1978) 159–191.

[20] S. Jia, J. Shan, Flexible structure vibration control using double-gimbal variable-speed control moment gyros, Journal of Guidance, Control, and Dynamics 44 (5) (2021) 954–966. https://doi.org/10.2514/1.G005684.

[21] C. Yang, K. Liang, Y. Rong, Q. Sun, A hybrid reduced-order modeling technique for nonlinear structural dynamic simulation, Aerospace Science and Technology 84 (2019) 724–733. https://doi.org/10.1016/j.ast.2018.11.008.

[22] K. Tsuchiya, T. Kashiwase, K. Yamada, Reduced-order models of a large flexible spacecraft, Journal of Guidance, Control, and Dynamics 12 (6) (1989) 845–850. https://doi.org/10.2514/3.20490.

[23] Q. Hu, Sliding mode attitude control with l2-gain performance and vibration reduction of flexible spacecraft with actuator dynamics, Acta Astronautica 67 (5-6) (2010) 572–583. https://doi.org/10.1016/j.actaastro.2010.04.018.

[24] R. Chai, A. Tsourdos, A. Savvaris, S. Chai, Y. Xia, C. P. Chen, Review of advanced guidance and control algorithms for space/aerospace vehicles, Progress in Aerospace Sciences 122 (2021) 100696. https://doi.org/10.1016/j.paerosci.2021.100696.

[25] J. Granda, L. Nguyen, Alternative Techniques for Developing Dynamic Analysis Computer Models of The International Space Station, Space Shuttle and Orbiter Repair Maneuvers, 2006. https://doi.org/10.2514/6.2006-2103.

[26] E. Alyaa, J. Granda, Modal analysis of the zvesda mission of the space station with bond graphs, in: Proceedings of the 2005 Internatinal Conference on Bond Graph Modeling and Simulation. New Orleans, 2005.

[27] G. Avanzini, E. Capello, I. A. Piacenza, Mixed newtonian-lagrangian approach for the analysis of flexible aircraft dynamics, Journal of Aircraft 51 (5) (2014) 1410–1421. https://doi.org/10.2514/1.C032235.

[28] L. Meirovitch, I. Tuzcu, Integrated approach to the dynamics and control of maneuvering flexible aircraft (2003).

[29] MSC, Patran 2021.4 - Online Help (HTML) (2021).
URL https://help.mscsoftware.com/bundle/patran_2021.4/page/patran_main.htm

[30] L. J. DeLucas, International space station, Acta astronautica 38 (4-8) (1996) 613–619. https://doi.org/10.1016/0094-5765(96)00056-2.

[31] J. E. Catchpole, The international space station: building for the future, Springer Science & Business Media, 2008.

[32] G. H. Kitmacher, W. H. Gerstenmaier, J.-D. F. Bartoe, N. Mustachio, The international space station: A pathway to the future, Acta astronautica 57 (2-8) (2005) 594–603. https://doi.org/10.1016/j.actaastro.2005.03.027.

[33] B. Wie, Space vehicle dynamics and control, Aiaa, 1998. https://doi.org/10.2514/4.860119.

[34] O. A. Bauchau, J. I. Craig, Euler-bernoulli beam theory, in: Structural analysis, Springer, 2009, pp. 173–221. https://doi.org/10.1007/978-90-481-2516-6_5.

[35] R. L. Bisplinghoff, H. Ashley, R. L. Halfman, Aeroelasticity, Courier Corporation, 2013. https://doi.org/10.1002/zamm.19560360764.

[36] G. Avanzini, F. Nicassio, G. Scarselli, Reduced-order short-period model of flexible aircraft, Journal of Guidance, Control, and Dynamics 40 (8) (2017) 2017–2029. https://doi.org/10.2514/1.G002387.

[37] D. Fattizzo, Reduced order model for attitude dynamics of a large flexible space structure, Ph.D. thesis, University of Salento, Lecce, Italy (2019).

[38] K. A. Ford, C. D. Hall, Singular direction avoidance steering for control-moment gyros, Journal of Guidance, Control, and Dynamics 23 (4) (2000) 648–656. https://doi.org/10.2514/2.4610.

[39] B. Wie, D. Bailey, C. Heiberg, Singularity robust steering logic for redundant single-gimbal control moment gyros, Journal of Guidance, Control, and Dynamics 24 (5) (2001) 865–872. https://doi.org/10.2514/2.4799.